8554 *Biochemistry* **2010,** *49,* 8554–8563
DOI: 10.1021/bi100913v

BIOCHEMISTRY
including biophysical chemistry & molecular biology
Article

Substitution of Ala for Tyr567 in RB69 DNA Polymerase Allows dAMP and dGMP To Be Inserted opposite Guanidinohydantoin[†,‡]

Jeff Beckman,[§] Mina Wang,[§] Gregor Blaha, Jimin Wang,* and William H. Konigsberg*

Department of Molecular Biophysics and Biochemistry, Yale University, New Haven, Connecticut 06520-8024.
[§]*These authors contributed equally to this work.*

Received June 7, 2010; Revised Manuscript Received August 19, 2010

ABSTRACT: Continuous oxidative damage inflicted on DNA produces 7,8-dihydro-8-oxoguanine (8-oxoG), a commonly occurring lesion that can potentially cause cancer by producing G → T transversions during DNA replication. Mild oxidation of 8-oxoG leads to the formation of hydantoins, specifically guanidinohydantoin (Gh) and spiroiminodihydantoin (Sp), which are 100% mutagenic because they encode almost exclusively the insertion of dAMP and dGMP (encoding G → T and G → C transversions, respectively). The wild-type (wt) pol α family DNA polymerase from bacteriophage RB69 (RB69pol) inserts dAMP and dGMP with low efficiency when situated opposite Gh. In contrast, the RB69pol Y567A mutant inserts both of these dNMPs opposite Gh with > 100-fold higher efficiency than wt. We now report the crystal structure of the "closed" preinsertion complex for the Y567A mutant with dATP opposite a templating Gh (*R*-configuration) in a 13/18mer primer-template (P/T) at 2.0 Å resolution. The structure data reveal that the Y to A substitution provides the nascent base pair binding pocket (NBP) with the flexibility to accommodate Gh by allowing G568 to move in the major-to-minor groove direction of the P/T. Thus, Gh is rejected as a templating base by wt RB69pol because G568 is inflexible, preventing Gh from pairing with the incoming dATP or dGTP base.

The average human cell acquires approximately 6000 DNA lesions per day because of oxidative damage by reactive oxygen species (ROS) (*1*). Guanine has the lowest oxidation potential of the four natural bases and is readily oxidized to 7,8-dihydro-8-oxoguanine (8-oxoG)[1] (*2*). As a templating base, 8-oxoG encodes insertion of dCMP and dAMP (Figure 1A). G → T transversions, which have been linked to cancer, aging, and other deleterious diseases, occur if a DNA polymerase mistakenly inserts dAMP opposite 8-oxoG that is in the *syn* conformation (*syn*-8-oxoG) (*3*−*5*).

8-oxoG has a lower oxidation potential than G (*6*−*8*) and can be oxidized further, forming a variety of lesions, such as guanidinohydantoin (Gh) and spiroiminodihydantoin (Sp) (Figure 1B) (*9*, *10*). These lesions can form a base pair between their hydantoin rings and dATP, although the most stable conformation of Gh is "*high-syn*", which would create a slightly "buckled" base pair with dATP (Figure 1C) (*11*, *12*). [For reference, Figure 1D shows the numbering scheme for Gh (*13*).] Gh and Sp do not base pair with dCTP, so these lesions are more mutagenic than 8-oxoG (*14*). Burrows et al. (*15*−*17*) confirmed this when they found that the Klenow fragment (KF) could insert dAMP, but not dCMP, opposite Gh and Sp. dGMP was also inserted opposite these lesions, albeit with an efficiency lower than that of dAMP. It has been proposed that the efficiency of dGMP insertion is higher than that of dCMP or dTMP because a G:Gh base pair is closer to "ideal" Watson−Crick geometry (*11*).

Misinsertion of dGMP gives rise to G → C transversions that have been identified with high frequency in cells that have been transformed with plasmids exposed to the following oxidizing agents: (i) UV light (*18*, *19*), (ii) hydrogen peroxide (*20*), (iii) methylene blue and light (*21*), and (iv) singlet oxygen (endoperoxide) (*22*). Although Gh has not been detected directly in cancer cells with elevated levels of these mutations, e.g., some head and neck carcinoma cell lines (*23*), hydantoins like Gh are one of only a few known DNA adducts formed by oxidation to encode G → C transversions, linking Gh and Sp to human cancer (*24*). This link was strengthened by the findings that Gh and Sp were substrates for removal by the mammalian glycosylases NEIL1, NEIL2, and hNEIL1 (*25*−*27*), suggesting that DNA repair pathways have evolved to recognize and excise hydantoins.

Unlike the situation with KF, Gh blocked replication by family B polymerases such as RB69pol, calf thymus DNA pol α, and human DNA pol β (*11*, *17*). A recently determined crystal structure of RB69pol in complex with DNA containing Gh revealed that the mechanism by which RB69pol rejected Gh as a

[†]Supported by U.S. Public Health Service Grant GM 063276-09.
[‡]With regard to author contributions, J.B. determined the kinetic parameters, M.W. crystallized and determined the structure of the RB69pol−Gh ternary complex, G.B. collected data at APS, and J.B., J.W., and W. H.K. helped to interpret the data, designed experiments, and contributed to writing the paper.
*To whom correspondence should be addressed: Department of Molecular Biophysics and Biochemistry, Yale University, SHM CE-14, New Haven, CT 06520-8114. Telephone: (203) 785-4599. Fax: (203) 785-7979. E-mail: william.konigsberg@yale.edu or jimin.wang@yale.edu.
[1]Abbreviations: Gh, guanidinohydantoin; Sp, spiroiminodihydantoin; 8-oxoG, 7,8-dihydro-8-oxoguanine; Tg, thymine glycol; tC^{o}, 1,3-diaza-2-oxophenoxazine; pols, DNA polymerases; wt, wild-type RB69pol; RB69pol, bacteriophage RB69 DNA polymerase; KF, *Escherichia coli* DNA polymerase I; NBP, nascent base pair binding pocket; dAP, 2-aminopurine; Pu, purine; Py, pyrimidine; Cα-H, methylene hydrogen atom of Gly; dNMP, deoxynucleoside monophosphate; dNTP, deoxynucleoside triphosphate; k_{obs}, observed rate constant; k_{pol}, maximum rate of dNMP insertion; $K_{d,app}$, dNTP concentration that supports the half-maximal rate of dNMP insertion; P/T, primer-template DNA duplex. PDB, Protein Data Bank.

 Published on Web 08/26/2010

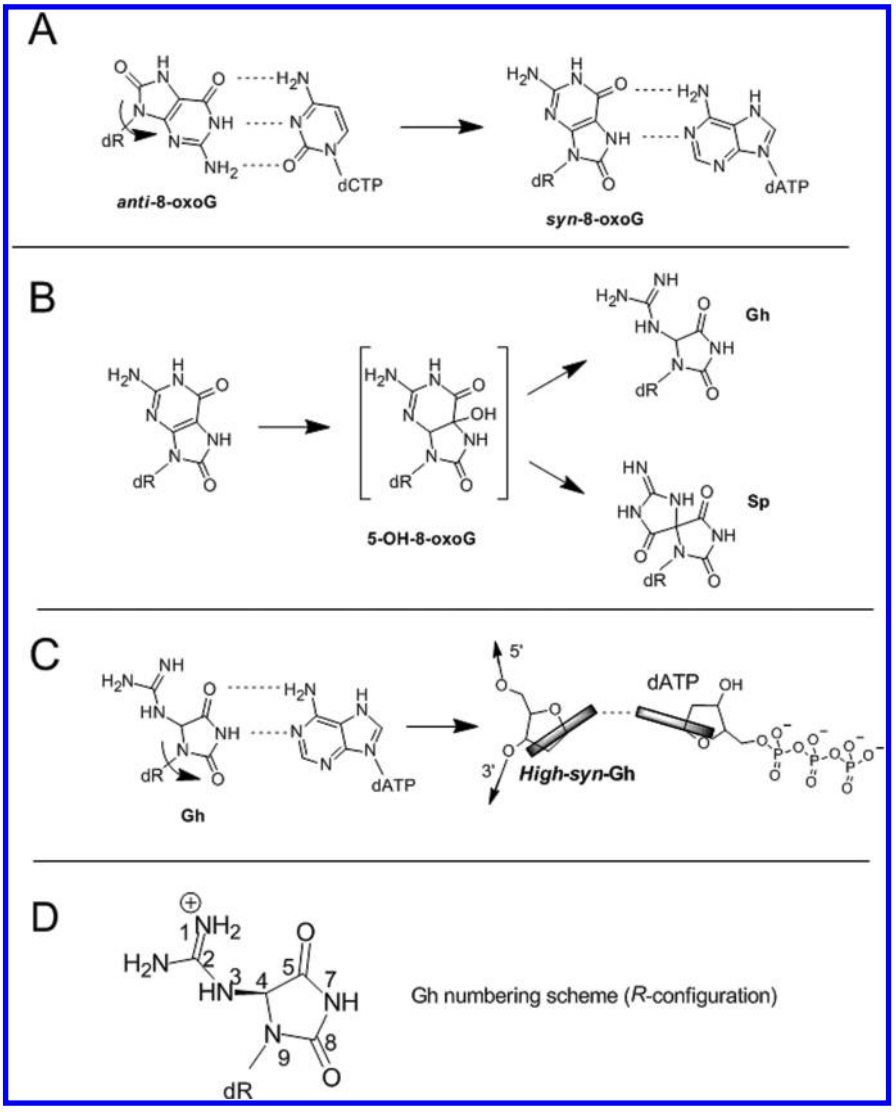

FIGURE 1: 8-oxoG compared with its oxidized products Gh and Sp. (A) Structures of an incoming dCTP or dATP paired opposite a templating 8-oxoG. (B) Hydantoin products of one-electron oxidation of 8-oxoG, Gh and Sp, via a 5-OH-8-oxoG intermediate. (C) Slight rotation of Gh relative to the 2′-deoxyribose sugar (indicated with a curved arrow) forms a base pair with dATP with Gh in a *high-syn* conformation. Note how the base pair buckles (the arrows pointing away from the Gh sugar indicate that the backbone continues in the 5′ and 3′ directions). (D) Numbering scheme of Gh, shown in the *R*-configuration at C-4.

templating base was by flipping it away from contact with an incoming dNTP and into the major groove (*11*). Because Gh has high mutagenic potential, and because RB69pol has a relatively high degree of sequence similarity to human pols α and δ (*28*), it was of interest to determine why wt RB69pol rejects Gh as a templating base. To do so, we would have to trap Gh in the templating position in a ternary complex.

We recently reported that the RB69pol Y567A mutant increased the insertion efficiency of dAMP opposite 8-oxoG by >2 orders of magnitude relative to that of wt (*29*). Figure 2 illustrates the location of Y567 in relation to the nascent base pair and other NBP residues. Replacement of the Y567 side chain with a methyl group increased the flexibility of the neighboring G568 residue, allowing it to readjust its position to accommodate, and stabilize, *syn*-8-oxoG (*29*). Because Gh has structural and chemical features similar to those of *syn*-8-oxoG in regions of the molecule that would closely contact G568 and the incoming dATP base, we predicted that the Y567A mutant would also be able to insert dAMP opposite Gh with high efficiency. This prediction was confirmed when we found that dAMP opposite Gh was incorporated

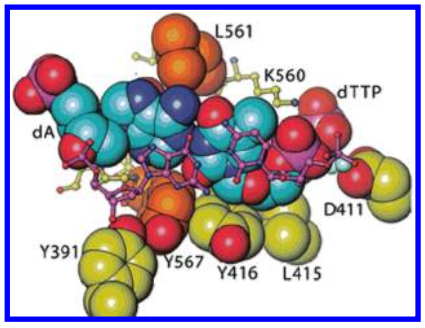

FIGURE 2: Steric relationship of some of the NBP residues surrounding an incoming dTTP paired opposite a templating dA (from ref *34*; PDB entry 1IG9). The nascent base pair and surrounding residues are shown from the duplex side of the P/T in space-filling form. The nascent base pair is colored blue, and the terminal C:G base pair is shown in stick form (purple) for the sake of clarity. L561 and Y567 are colored orange.

with a >200-fold greater efficiency than wt. In addition, the insertion efficiency of dGMP opposite Gh by the Y567A mutant

Table 1: Primer-Template Sequences Used in This Study[a]

GCGGACTGCTTAC-dd GCGCCTGACGAATG**G$_h$**ACT	**D$_{GH}^{dd}$**
GCGGACTGCTTAC GCGCCTGACGAATG**X**ACT	**D$_X$** (X = Gh, 8-oxoG, Tg, or tC^o)
GCGGACTGCTTACC GCGCCTGACGAATGG$_o$**A**CT	**D$_{C:OG}$**
GCGGACTGCTTACA GCGCCTGACGAATGX**A**CT	**D$_{A:X}$** (X = Gh, 8-oxoG, Tg, or tC^o)
GCGGACTGCTTACG GCGCCTGACGAATGX**A**CT	**D$_{G:X}$** (X = Gh, Tg, or tC^o)

[a]The templating base is in bold. G_o is 8-oxoG, and G_h is guanidinohydantoin (Gh). D_{GH}^{dd} was used to grow crystals of the ternary complex.

increased by 100-fold relative to that of wt. To provide the structural basis for efficient utilization of Gh as a templating base by the Y567A mutant, and in an attempt to understand why wt RB69pol cannot bypass Gh, we determined the crystal structure of the ternary complex of the Y567A mutant with dATP opposite a templating Gh at 2.0 Å resolution. Our kinetic and structural data have provided insights into how dATP and dGTP are utilized by the Y567A mutant when paired opposite Gh and have led to a deeper understanding of base selectivity, as discussed below.

MATERIALS AND METHODS

Materials. Materials and reagents were of the highest quality commercially available. dNTPs were purchased from Roche (Burgess Hill, U.K.); T4 polynucleotide kinase was purchased from New England Biolabs (Ipswich, MA), and [γ-^{32}P]ATP was purchased from MP Biomedicals (Irvine, CA).

Enzymes. Wild-type RB69pol and the Y567A mutant, in an exonuclease-deficient background (D222A and D327A), were overexpressed in *Escherichia coli*, purified, and stored as previously described (*30*).

DNA Substrates. Sequences of P/T's used in this study are listed in Table 1. Oligonucleotides, with the exception of those containing Gh, were synthesized at the Keck facilities (Yale University). Oligonucleotides containing 8-oxoG were oxidized with Ir(IV) to convert 8-oxoG to the two diastereoisomers of Gh as described previously (*15*, *16*). Primers were labeled on the 5′-end with ^{32}P using T4 polynucleotide kinase and [γ-^{32}P]ATP (except when used for crystallography) and annealed to unlabeled templates as previously described (*31*, *32*).

Chemical Quench Experiments. Rapid chemical quench experiments were performed at 23 °C with a buffer solution of 66 mM Tris-HCl (pH 7.4) using a Kintek RFQ-3 instrument. For k_{pol} and $K_{d,app}$ determinations, single-turnover conditions were used with a 10-fold excess of RB69pol over P/T. Briefly, the enzyme and P/T from one syringe were rapidly mixed with Mg^{2+} and various dNTP concentrations from the other syringe for times ranging from 5 ms to 1 min. For reactions that required longer times, experiments were performed manually on the benchtop. For most reactions, the rate of phosphoryl transfer was too slow to obtain kinetic parameters in the presence of a trap, e.g., cold dsDNA or heparin. However, in the case of insertion of dAMP opposite Gh by the Y567A mutant, where the rate of chemistry was orders of magnitude faster than the rate of DNA release, 10×[cold P/T]/[enzyme] was used to ensure that single-turnover conditions were met (Table 2). The final concentrations after mixing were as follows: 1 μM enzyme, 90 nM ^{32}P-labeled P/T, and 10 mM Mg^{2+}. Reactions were quenched with 0.5 M EDTA (pH 8.0). Substrates and products were separated by PAGE [19:1 (w/v) acrylamide/bisacrylamide gels containing 8 M urea], visualized using a STORM imager (Molecular Imaging), and quantitated using Imagequant (GE Healthcare) and GraphPad Prism.

Table 2: Pre-Steady-State Kinetic Parameters for Insertion of dNMPs opposite Gh by Wild-Type RB69pol and Its Y567A Mutant

enzyme	dNTP	template	k_{pol} (s^{-1})	$K_{d,app}$ (μM)	$k_{pol}/K_{d,app}$ (μM^{-1} s^{-1})
wild type	dATP	Gh	ND[a]	ND[a]	2.0×10^{-3}
	dGTP	Gh	ND[a]	ND[a]	5.7×10^{-5}
Y567A	dATP[b]	Gh	300	760	0.39
	dGTP	Gh	4.8	1400	3.4×10^{-3}

[a]ND = Not determined because the value of $K_{d,app}$ was too high (>2 mM). [b]Progress curves were biphasic. Values shown are from the fast phase that comprised 80% of the product formed (see the text). The $k_{pol}/K_{d,app}$ second-order value was obtained by calculating the slope of a line for which $y = mx + b$, where m is the slope ($= \Delta k_{obs}/\Delta[dNTP] = k_{pol}/K_{d,app}$). Of the values shown, standard deviations were within 10−20 and ~30% for k_{pol} and $K_{d,app}$ values, respectively.

Data Analysis. The amount of product formed versus time for each dNTP concentration was fitted by nonlinear regression to the general form of eq 1 to yield observed rates of product formation, k_{obs}:

$$Y = \sum_{i=1}^{n} A_i e^{-k_i t} + C \quad (1)$$

where Y is the concentration of the DNA product formed during the reaction, C is the offset constant, A_i is the observed amplitude of product formation, and k_i is the observed rate constant. The kinetic parameters k_{pol} (the rate of phosphoryl transfer) and $K_{d,app}$ (defined as the dNTP concentration at which the rate of phosphoryl transfer reaches $^1/_2 k_{pol}$) were obtained by plotting k_{obs} versus dNTP concentration to eq 2:

$$k_{obs} = \frac{k_{pol}[dNTP]}{K_{d,app} + [dNTP]} \quad (2)$$

where k_{obs} represents the observed rate at a given dNTP concentration. Note that the $K_{d,app}$ values are not ground-state dissociation constants for dNTP binding. This is because the observed dNTP concentration dependence of rates of product formation is affected by steps such as the reversible conformational change that occurs subsequent to dNTP binding but prior to phosphoryl transfer.

Crystallization of RB69pol Y567A Mutant Ternary Complexes with dATP and Gh. D_{GH}^{dd} was used for crystallization (Table 1). The primer was dideoxy-terminated to prevent nucleotide incorporation. The RB69pol Y567A mutant (final concentration of 110 μM) was mixed with an equimolar ratio of freshly annealed D_{GH}^{dd}. dATP was then added to a final concentration of 3.7 mM. Using microbatch vapor-diffusion methods, a solution of 150 mM $CaCl_2$, 15% (w/v) PEG 350 monomethyl

Table 3: Crystallographic Data and Refinement Statistics of the Y567A−dATP−Gh Complex

space group	$P2_12_12_1$
unit cell dimensions [a, b, c (Å)]	75.013, 119.783, 130.727
resolution range (Å)	50.00−2.00 (2.07−2.00)[a]
wavelength (Å)	1.10000
no. of unique reflections	74483 (5982)[a]
redundancy	4.5 (3.2)[a]
completeness (%)	93.2 (75.8)[a]
R_{merge} (%)[b]	7.8 (> 100)[a]
I/σ	14.3 (0.96)[a]
Refinement Statistics	
no. of reflections	69794
R_{work} (%)[c]	19.4
R_{free} (%)[d]	23.1
final model	
no. of non-hydrogen atoms	8925
no. of amino acid residues	903
no. of water molecules	705
no. of Ca^{2+} ions	4
no. of template nucleotides	18
no. of primer nucleotides	13
no. of dNTP molecules	1
average B factor (Å^2)	
protein	27.3
waters	34.3
rmsd[e]	
bond lengths (Å)	0.0069
bond angles (deg)	1.106
PDB entry	3NAE

[a]The highest-resolution shell statistics are given in parentheses. [b]$R_{merge} = \langle\sum_{hkl}\sum_j|I_j(hkl) - \langle I(hkl)\rangle|\rangle/\langle I(hkl)\rangle$, merging statistics for all symmetry mates. [c]$R_{work} = \sum_{hkl}||F_{obs}(hkl)| - |F_{calc}(hkl)||/\sum_{hkl}|F_{obs}(hkl)|$ (crystallographic R factor). [d]R_{free} is the cross-validation R factor for ~5% of the total unique reflections that were omitted. [e]Root-mean-square deviation from ideal values.

ether (MME), and 100 mM sodium cacodylate (pH 6.5) was mixed with an equal volume of the Y567A−D_{GH}^{dd}−dATP complex. Crystals typically grew in 3 days at 20 °C with dimensions of ~70 μm × ~50 μm × ~50 μm. Crystals were transferred from the mother liquor to a cryoprotectant/precipitant stabilization solution containing 20% (w/v) PEG 350 MME, 100 mM $CaCl_2$, and 100 mM sodium cacodylate (pH 6.5), and then to a stabilization solution with the level of PEG 350 increased to 30% (w/v) as a cryoprotectant prior to being frozen in liquid nitrogen.

Data Collection, Structure Determination, and Refinement. X-ray diffraction data were collected using synchrotron radiation sources at beamline X25 at the National Synchrotron Light Source (Brookhaven National Laboratory, Upton, NY) at a wavelength of 1.10000 Å and at 110 K using synchrotron radiation sources. The crystal belonged to orthorhombic space group $P2_12_12_1$ with different unit cell parameters (Table 3). Data were processed using the HKL2000 program suites (*33*).

Starting with the pol structure from the ternary complex of wt RB69pol without the P/T duplex or dNTP (*34*), the structure was determined by molecular replacement using AMORE (*35*) and refined using REFMAC5 (*36*). The P/T duplex and dNTP were built into electron density maps using COOT (*37*). The incoming dATP binds two Ca^{2+} ions at the A and B metal ion sites, which was observed previously (*34*). The structure of Gh was derived from PDB entry 3L8B, which contains a Gh nucleotide residue in the template strand (*11*). Structure refinement statistics are listed in Table 3. Figures obtained from the crystal structures were created using Ribbons (*38*).

PDB Entries. Coordinates and structure factors for the Y567A mutant−dATP−Gh ternary complex structure have been deposited in the PDB as entry 3NAE.

RESULTS

Insertion of dNMPs opposite Gh by Wild-Type RB69pol and the Y567A Mutant. Overall, bypass of a Gh lesion by a replicative DNA pol is much more mutagenic than bypass of 8-oxoG, because Gh does not base pair with dCTP (Figure 3A) (*9*). Steady-state kinetic analysis of incorporation of dNMP opposite Gh by wt RB69pol showed that this lesion allows insertion of dATP and dGTP, but with very low efficiency (*11*). Under pre-steady-state conditions, insertion of dAMP and dGMP opposite Gh by wt RB69pol occurred with efficiencies of 1.5×10^{-3} and 5.7×10^{-5} μM^{-1} s^{-1}, respectively, favoring insertion of dAMP over dGMP by 25-fold. These efficiencies are still ~3000-fold lower than that for the insertion of correct dNMPs by wt opposite an undamaged templating base (Table 2) (*39*).

What prevents incorporation of dAMP and dGMP opposite Gh by wt RB69pol? We had previously found that the Y567A mutant increased the efficiency of incorporation of dAMP opposite *syn*-8-oxoG by 3 orders of magnitude relative to that of wt (*29*). We speculated that this may have occurred in part because the Y to A substitution provides G568 with the flexibility to accommodate *syn*-8-oxoG, as well as its ability to form a potentially stabilizing hydrogen bond between the Cα hydrogen atom of G568 and the O-8 carbonyl oxygen of 8-oxoG (*29*). As with *syn*-8-oxoG, Gh contains a carbonyl oxygen that is close enough to the Cα hydrogen of G568 to form a hydrogen bond. This suggested that Y567A would also increase the efficiency of incorporation of dAMP opposite Gh as it does with dAMP opposite 8-oxoG. Under pre-steady-state conditions in the presence of a cold DNA trap (see Materials and Methods), the progress curves for the Y567A mutant inserting dAMP opposite Gh occurred in two phases: a fast phase accounting for approximately 80% of the total product formed and a slow phase responsible for the remainder. Because Gh exists as a racemic mixture of diastereoisomers, differing only at the C-4 atom that links the hydantoin ring with the guanidinium group (Figure 1D) (*11*), the biphasic curves may represent insertion of dAMP opposite each of the two forms. Analysis of the "fast" phase revealed that dAMP insertion efficiency was 200 times greater than that observed with wt RB69pol (Figure 3). The k_{pol} is similar to the rate of insertion of dCMP opposite G (Table 2) (*39*). dGMP incorporation efficiency, when opposite Gh, by the Y567A mutant also increased 100-fold versus that of wt (Table 2).

Extension past A:Gh and G:Gh Base Pairs. Bypass of A:Gh and G:Gh terminal base pairs by wt RB69pol and the Y567A mutant was very inefficient (10^5−10^6-fold slower than extension past normal Watson−Crick base pairs) (Table 4). By comparison, the bypass efficiency of terminal C:8-oxoG and A:8-oxoG base pairs by both wt RB69pol and the Y567A mutant (*29*) was at least 3 orders of magnitude more efficient than extension past A:Gh and G:Gh base pairs (Table 4).

Bypass of Other Template Analogues. For further insight into why the Y567A mutant efficiently bypassed 8-oxoG but not Gh, we examined the ability of wt RB69pol and the Y567A mutant to bypass thymine glycol (Tg) and 1,3-diaza-2-oxophenoxazine (tC^o) (Figure 4). Previous results had shown that wt RB69pol bypass of Tg was very inefficient, but that bypass of tC^o by the related B family human pol α was highly efficient (*40*, *41*).

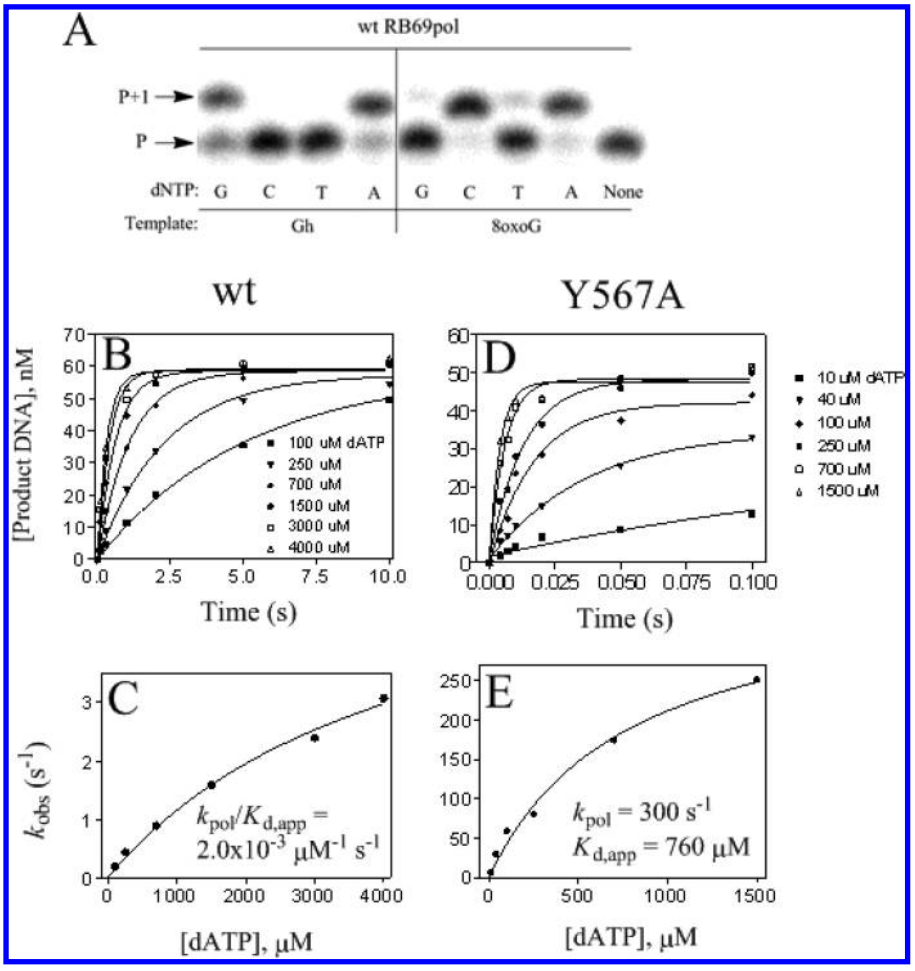

FIGURE 3: Kinetics of dNMP insertion by wt RB69pol and the Y567A mutant. (A) Insertion of dNMPs opposite Gh and 8-oxoG by wt RB69pol. P represents the primer, and P+1 represents the primer extended by one nucleotide. Oxidation of 8-oxoG to Gh results in a dramatically reduced level of incorporation of dCMP, to the point that it cannot be observed. (B) Kinetics of insertion of dAMP opposite Gh by wt. Progress curves at various dATP concentrations fit to single-exponential equations. (C) Plot of k_{obs} vs dATP concentration fit to eq 2. (D) Kinetics of insertion of dAMP opposite Gh by the Y567A mutant. Same as panel B but with data obtained using the Y567A mutant. (E) Same as panel C using the results from panel D.

Table 4: Kinetic Parameters for the Insertion of Correct dNMPs past Terminal Base Pairs Containing Gh or 8-oxoG

		wt RB69pol			Y567A		
dNTP	P/T	k_{pol} (s^{-1})	$K_{d,app}$ (μM)	$k_{pol}/K_{d,app}$ (μM^{-1} s^{-1})	k_{pol} (s^{-1})	$K_{d,app}$ (μM)	$k_{pol}/K_{d,app}$ (μM^{-1} s^{-1})
dTTP	$D_{A:GH}$	ND[a]	ND[a]	1.3×10^{-5}[b]	0.067	1700	3.9×10^{-5}[b]
	$D_{G:GH}$	ND[a]	ND[a]	1.6×10^{-6}[b]	ND[a]	ND[a]	4.6×10^{-5}[b]
	$D_{A:OG}$[c]	ND[a]	ND[a]	1.2×10^{-2}[b]	200	850	0.31
	$D_{C:OG}$[c]	ND[a]	ND[a]	5.0×10^{-3}[b]	230	740	0.24

[a]Not determined because the value of $K_{d,app}$ was too high (> 2 mM). [b]The $k_{pol}/K_{d,app}$ second-order value was obtained by calculating the slope of a line fitted to the data: $y = mx + b$ (see Table 2). [c]Data obtained previously (*29*). Standard deviations were within the same range as those of the data presented in Table 2.

Both wt RB69pol and the Y567A mutant rapidly inserted dAMP opposite Tg, and dGMP opposite tC°, and both pols rapidly inserted the next correct dNMP (dTMP) past terminal G:tC° and A:tC° base pairs, but only slowly extended past A:Tg and G:Tg base pairs. In most cases, compared to wt, the Y567A mutant increased the rate of bypass by at least several-fold.

Crystal Structure of the Y567A Mutant in a Complex with a Dideoxy P/T Containing a Templating Gh opposite dATP. To correlate kinetics with structure, we required high-quality crystals of RB69pol with a templating Gh. Recently, a crystal structure of wt RB69pol in complex with ddP/T containing Gh was reported (*11*). Surprisingly, although Gh was expected to be in the templating position, it was flipped out into the major groove. Also, despite having been grown in a solution containing 10 mM ddATP under conditions that would allow phosphoryl transfer, no electron density was observed for an inserted ddAMP, and the polymerase remained in an "open" conformation (*11*). We have determined the structure of a ternary complex of the Y567A mutant with a templating Gh opposite dATP, at 2.0 Å resolution with an R_{free} value of 23% (Table 3). In contrast to the reported wt RB69pol−Gh complex, Gh in the Y567A mutant structure is paired opposite dATP in the "closed"

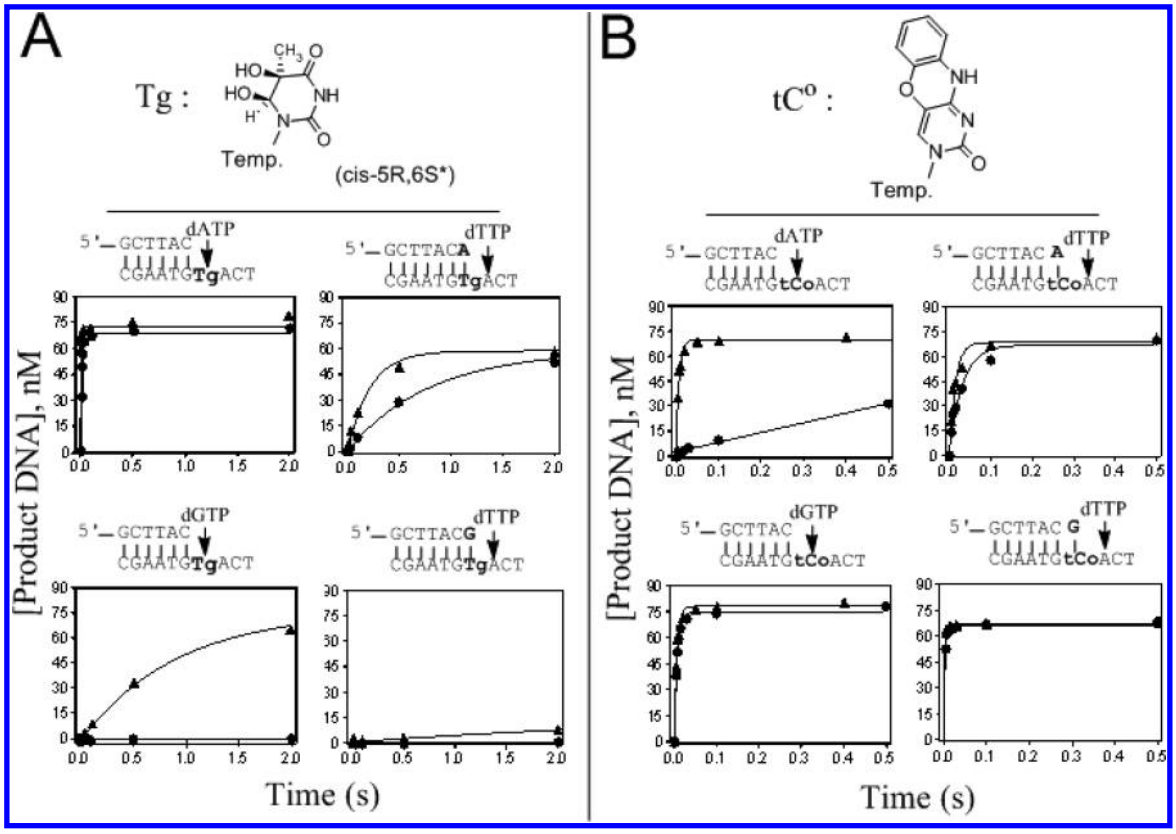

FIGURE 4: Progress curves showing the rates of bypass of thymine glycol (Tg) and 1,3-diaza-2-oxophenoxazine (tC°) by wt RB69pol and the Y567A mutant. For reference, P/T sequences and structures of the analogues are shown. Progress curves for insertion of dNMPs were obtained with 10-fold excess enzyme over P/T, and with 1 mM dNTPs (see Materials and Methods). (A) Rate of DNA product formation for insertion of dAMP and dGMP opposite Tg, and extension past A:Tg and G:Tg base pairs (via insertion of dTMP, the next correct dNMP), by wt RB69pol (●) and the Y567A mutant (▲). (B) Rate of DNA product formation for insertion of dAMP and dGMP opposite tC°, and extension past A:tC° and G:tC° base pairs, by wt RB69pol (●) and the Y567A mutant (▲). The asterisk indicates that after oligonucleotide synthesis and deprotection, Tg is predominantly in the *cis*-5*R*,6*S* configuration (*40*).

conformation with the hydantoin ring of Gh forming a hydrogen bond between N-7 of Gh and N-1 of dATP (Figure 5). Although we predicted that O-5 of Gh and N-6 of dATP would have the ability to form an interbase hydrogen bond, this did not occur. Instead, O-5 of Gh and N-6 of dATP form an indirect hydrogen bond mediated by an ordered water molecule (Figure 5A). The electron density of the guanidinium group of Gh was well-resolved. As was the case in the wt binary structure, Gh, which has a chiral center at C-4 and exists as a mixture of *S*- and *R*-forms, was found exclusively in the *R*-configuration. (Computer modeling showed that if the *S*-configuration would have been captured instead, the guanidinium moiety would have pointed toward the helix P side chains, which would force the 3′-template base of a nascent base pair to buckle to avoid steric repulsion.)

For insight into the structural consequences of having a templating Gh in the NBP, we superimposed the palm domains of ternary complexes of wt with the dCTP:dG base pair and the Y567A mutant with the dATP:Gh base pair (Figure 5B). The wt structure was determined at 1.8 Å resolution (M. Wang, manuscript in preparation). We observed that the incoming dATP was almost perfectly superimposed onto the incoming dCTP in the wt RB69pol structure, although the orientation of the glycosidic bond of the two incoming dNTPs differed slightly. The most significant changes in these structures were (i) the backbone of G568 being retracted into the DNA minor groove by 0.8 Å; (ii) the side chain of K279 being displaced by 6.7 Å to avoid a steric clash with the guanidinium moiety of Gh; and (iii) the vacated space, due to the Y567 to A substitution, being occupied by two ordered water molecules (data not shown).

DISCUSSION

To help counter the effects of oxidized DNA damage, it is important to understand the mechanism(s) by which DNA pols replicate DNA containing oxidized lesions like Gh. Recently, a wt RB69pol−P/T binary crystal structure was determined with the *R*-form of Gh at the P/T junction in the template strand (*11*). In contrast to the situation with the Y567A mutant, Gh shifted from the templating position into the major groove. However, wt RB69pol preferably inserts, albeit inefficiently, dAMP and dGMP opposite Gh, indicating that *R*-Gh rotates only infrequently into the templating position. Alternatively, only the *S*-form of Gh, which did not crystallize but is present in solution, can be positioned as a template base (*11*). Because *R*-Gh fits into the templating position nicely within the Y567A mutant closed ternary complex and maintains a preference for insertion of dAMP and dGMP opposite Gh, the likely mechanism utilized by the Y567A mutant to efficiently insert dAMP and dGMP is to increase the probability of repositioning Gh as the template base (Table 2 and Figure 5A). What structural feature does the Y567A mutant provide so that Gh can occupy the templating position? The Y567 Cα atom is ~11.3 Å from the guanidinium moiety, so the Y567 to A substitution cannot have a direct effect on the stability of Gh, i.e., by providing additional space in the NBP. Instead, the effect must be indirect. The loss of the phenolic side

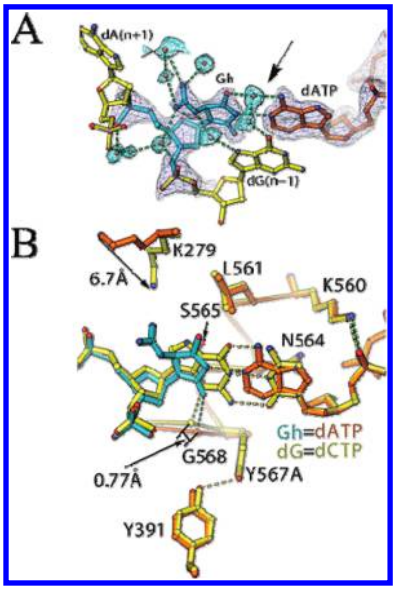

FIGURE 5: Crystal structure of the RB69pol Y567A mutant in a complex with a dATP:Gh base pair and its relationship to residues in the NBP. (A) Omitted $F_o - F_c$ electron density map of the dATP:Gh nascent base pair. Note the number of water molecules that surround the guanidinium group, and the water-mediated hydrogen bonding network that links Gh and dATP (denoted with an arrow). (B) Comparison of the crystal structures of wt and the Y567A mutant in a complex with dCTP:dG and dATP:Gh base pairs, respectively. Superimposed palm domains show that the Y567A substitution resulted in a shift of G568 into the DNA minor groove by ~0.8 Å. The wt−dCTP−dG backbone and base pair are colored yellow, and the Y567A−dATP−Gh backbone is colored orange. The dCTP:dG base pair is colored yellow, and the dATP:Gh base pair is shown with dATP colored orange and Gh colored blue.

chain of Y567 increases the flexibility of G568, thus stabilizing Gh as the templating base. Specifically, formation of a dATP:Gh base pair in the Y567A mutant can occur because G568 can move ~0.8 Å into the DNA minor groove to provide the space needed for Gh to pair with the base of dATP (Figure 5B). We had previously shown that the Y567A mutant is permissive for insertion of dAMP opposite *syn*-8-oxoG using the same mechanism (*29*). This increased flexibility also allows Gh to stabilize the dATP:Gh pair because the Cα hydrogen atom of G568 and O-8 of Gh are close enough for a hydrogen bond to form.

Currently, we do not fully understand why the substitution of the phenolic side chain of Y567 with a methyl group leads to more flexibility of G568. Because Y567 forms hydrogen bonds with Y391 and T587 and forms a close association with Y416, we suspect Y567 makes G568 rigid because Y567 is itself rigid. Thus, any, if not all, of the interactions formed between Y567 and other side chains may contribute to the rigidity of G568. We are currently in the process of analyzing the appropriate mutants to determine which interactions between side chains lead to increased G568 flexibility. Having a better understanding of how to increase the flexibility of active site residues would have practical applications, specifically in the field of protein engineering. In recent years, researchers have been synthesizing DNA with a variety of nucleotide modifications (e.g., refs (*42*−*47*)), aimed at the expansion of the genetic code and discovery of novel nucleic acid therapeutics (*48*). Theoretically, mutants could be engineered to have enough active site flexibility for judicious, and efficient, incorporation of novel base analogs into DNA.

Interestingly, despite the absence of stabilizing interactions between residues in the NBP and the guanidinium group of Gh, Gh is surprisingly well ordered and surrounded by five water molecules in an extended hydration network (Figure 5A). Numerous other ordered water molecules line the DNA major groove, including one mediating the interaction between O-5 of Gh and N-6 of dATP. This water molecule interacts with another water molecule in the major groove that binds to O-6 of the dG base that is 3′ to Gh on the templating strand (Figure 5A). With the exception of the mediation of water molecules between the nascent base pair, dATP binding opposite Gh suggests "normal" solvation and Watson−Crick-like base pairing. However, because the $K_{d,app}$ of dAMP insertion is approximately 15-fold higher than would be expected for a Watson−Crick base pair, it suggests that the apparent binding affinity of dATP is relatively low with the Y567A mutant (*39*) (Table 2). These kinetic observations correlate with the inability of the nascent base pair to form two strong interbase hydrogen bonds. Additionally, we have noted that the K279 side chain has shifted away from the guanidinium group of Gh by 6.7 Å probably because of electrostatic repulsion (Figure 5B). However, previous studies with the K279A mutant showed that K279 does not influence the insertion efficiency of dAMP opposite Gh (*11*). Despite the increase in $K_{d,app}$ for dATP, the k_{pol} is very high for dAMP insertion (300 s^{-1}), so presumably the dATP:Gh base pair is still optimally aligned for phosphoryl transfer (Table 2), consistent with the observation that dATP opposite Gh in this complex is superimposed well with dCTP opposite dG in the ternary complex structure (Figure 5B).

The dGTP:Gh Base Pair Adopts a "Wobble" Configuration in the Y567A Mutant Ternary Complex. It has been proposed that Gh pairs opposite G in a wobble configuration (*49*), where Gh acts like dT in terms of the interbase hydrogen bonding pattern. Modeling and NMR structural studies of duplex DNA have shown that base pairs adopt wobble configurations when interbase hydrogen bonds have the potential to form, suggesting that wobble pairing represents a possible mechanism for misinsertion of dNMPs by DNA pols (e.g., refs (*50*−*53*)). With an increase in the volume of the NBP in RB69pol, Klentaq1, and Taq pol1 by site-directed mutagenesis, dTMP insertion was 1−2 orders of magnitude more efficient opposite dG, suggesting that wt DNA pols use steric hindrance to prevent the formation of dTTP:dG wobble configurations (*39*, *54*, *55*). Specifically, the Y567A mutant inserts dTMP 40-fold more efficiently than does wt RB69pol. However, base pairing of dTTP opposite dG with two hydrogen bonds would require a wobble configuration, with the incoming base shifted into the DNA major groove, not downward into the space provided by the Y567 to A substitution. Thus, steric repulsion does not adequately explain how misinsertion of dTMP opposite dG is prevented in wt pol. Instead, the more efficient insertion of dTMP opposite dG by the Y567A mutant is likely caused by the increased flexibility of G568, allowing the templating dG to shift into the DNA minor groove (Figure 6A). In contrast, to obtain two interbase hydrogen bonds between dGTP and Gh, an "inverted wobble" configuration would be required, with the dGTP base shifting into the DNA minor groove (Figure 6B). In this case, a steric clash with Y567 would be a more probable explanation for why the wt pol rejects dGTP opposite Gh. We have recently determined the structures of two ternary complexes of the Y567A mutant with dTTP:dG and dCTP:2-aminopurine (dCTP:dAP) mispairs and found that the base pairs are in the wobble and inverted wobble configurations, respectively (W. H. Konigsberg, manuscript in preparation). The latter configuration

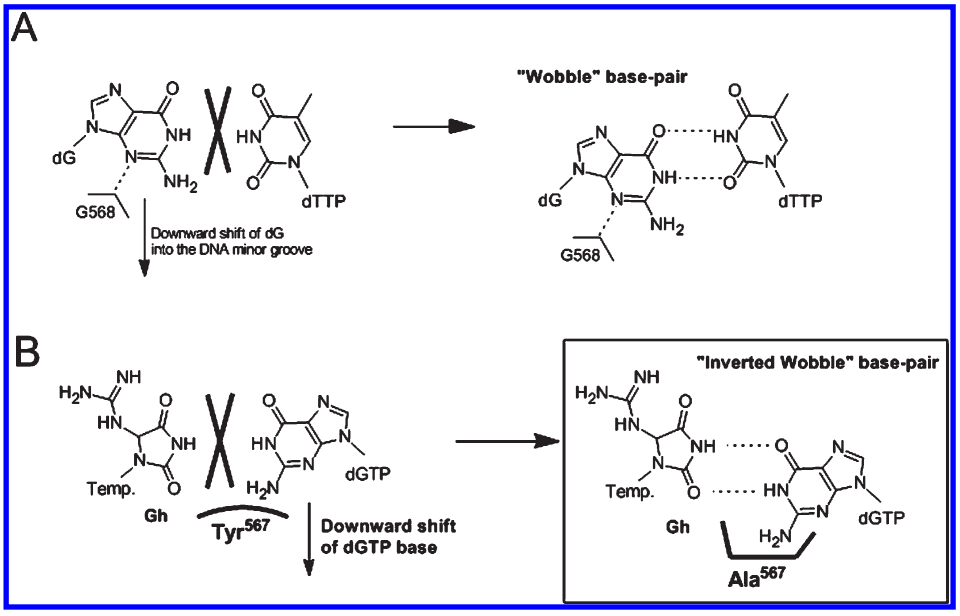

FIGURE 6: Possible wobble configurations of the dTTP:dG and dATP:Gh mispairs in the Y567A mutant complex. (A) Downward shift of dG into the DNA minor groove on the templating side (against G568) leads to a wobble base pair between dG and dTTP. (B) Downward shift of dGTP into the DNA minor groove into the space provided by the Y567 to A substitution leads to an inverted wobble base pair between dGTP and Gh.

leads to the formation of two hydrogen bonds between dCTP and dAP, with the base of dCTP shifted into the DNA minor groove and into the space provided by the Y567 to A substitution, just as we suspect happens with a dGTP:Gh pair (J. Wang, personal communication). Overall, the structural and kinetic data support our proposal that the dNTP or the templating base can readily be repositioned within the NBP of the Y567A mutant for formation of relatively stable mispairs.

Extension past A:Gh and G:Gh Base Pairs Is Blocked in both wt and the Y567A Mutant. Previous studies have shown that DNA pols, with the exception of KF, extend primers beyond terminal base pairs containing Gh with very low efficiency (*11*, *17*). Overall, with wt RB69pol, this makes Gh a very poor template for dNMP insertion as well as a very poor base-pairing partner for further extension of the growing primer strand. Interestingly, although the Y567A mutant is able to efficiently insert dAMP opposite Gh relative to wt, it is only slightly better (3-fold) at inserting the next correct dNMP past a dAMP:Gh terminal base pair than wt (Table 4). In contrast, the Y567A mutant efficiently conducts extension past dAMP:*syn*-8-oxoG and dCMP:*anti*-8-oxoG terminal base pairs, compared to wt, and this may provide an explanation for the Gh extension results (*29*). Modeling studies have shown that 8-oxoG in either the *syn*- or *anti*-orientation contains functional groups that would protrude into the pol cavity that holds the DNA duplex and would sterically clash with neighboring side chains, e.g., W574 and N572 (Figure 7A), so it is not surprising that wt RB69pol would be unable to efficiently bypass base pairs containing 8-oxoG (*29*, *56*). This proposal is supported by reports from the groups of Kool, Kuchta, and Romesberg (*57*−*61*), who have shown, using nucleoside analogues, that terminal base pairs have to adopt a Watson−Crick or similar geometry for efficient extension. The Y567A mutant may provide the flexibility for extension past protruding functional groups during DNA translocation through the pol active site by eliminating hydrogen bonds that would otherwise form a rigid network among Y567, Y391, and T578 (*29*, *62*). Because of this putative flexibility, the Y567A mutant should conduct extension past the dAMP:Gh and dAMP:*syn*-8-oxoG terminal base pairs with similar efficiencies. This is based on in silico modeling of A:Gh or A:*syn*-8-oxoG base pairs superimposed onto the terminal base pair (via the glycosidic bonds), which shows that similar steric clashes occur between Gh or 8-oxoG and its 5′-bridging phosphate group (Figure 7B, C) (*29*). However, the aforementioned terminal dAMP:Gh base pair is extended poorly relative to the dAMP:*syn*-8-oxoG base pair. This may be explained if we were to assume that Gh prefers to form a dAMP:*high-syn*-Gh configuration when in the terminal base pairing position. This configuration is predicted to be the most stable for Gh in DNA alone (*11*). A dAMP:*high-syn*-Gh base pair would create more distortion than a dAMP:Gh base pair because the former would buckle (see Figure 1C for a probable configuration of a dAMP:*high-syn*-Gh base pair). This distortion would be expected to cause steric repulsion with the adjacent nascent base pair and would lead to destabilization that would favor dNTP dissociation over phosphoryl transfer. Predictably, this repulsion could not be relieved by the additional flexibility of side chains in the Y567A mutant that protrude into the DNA minor groove.

Additional evidence that supports the idea that Watson−Crick or similar geometry is required for efficient bypass is provided by the observation that the Y567A mutant rapidly extends past a G:tC^{o} terminal base pair, but much more slowly past an A:Tg base pair (Figure 4). Unlike tC^{o}, Tg, as with *high-syn*-Gh, distorts the terminal base pair plane in a fashion that prevents the 3′-templating base from forming a stable interaction with the dNTP (*40*). Presumably, bypass of tC^{o} is efficient because tC^{o} can form a Watson−Crick base pair, albeit with extra bulk protruding into the DNA major groove (Figure 4B) (*41*).

In summary, wt RB69pol is able to prevent misinsertion largely because it possesses a rigid DNA minor groove "wall", comprising Y567 and G568, that prevents not only misinsertion of dAMP opposite Gh but also misinsertion of dNMPs that could form Py:Pu, Pu:Py, or dGTP:Gh wobble pairs. Simply via substitution of Y567 with Ala, the fidelity drops dramatically

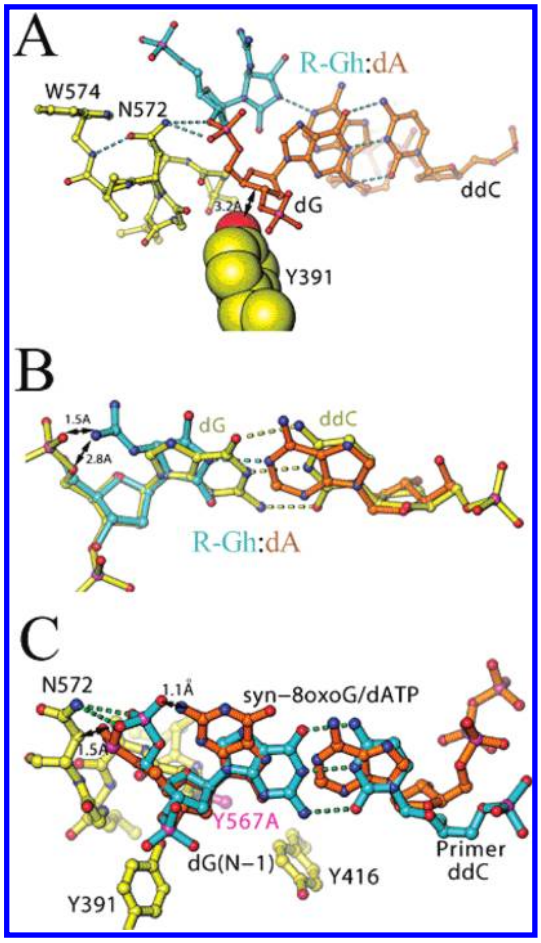

FIGURE 7: In silico modeling of a dAMP:Gh base pair as a terminal ($n - 1$) base pair and its relationship to surrounding amino acid side chains in the Y567A mutant. (A) Terminal ddC:dG base pair in the Y567A−dATP−Gh complex (orange) and the hydrogen bonding network it forms between the 5′-bridging phosphate of dG and side chains N572 and W574. (B) Superposition of the glycosidic bonds of the dATP:Gh base pair onto the ddC:dG base pair. Black arrows denote unfavorable interactions. (C) Superposition of the dATP:*syn*-8-oxoG base pair onto the ddC:dG base pair. Black arrows denote unfavorable interactions (*29*). Note that both Gh and *syn*-8-oxoG form unfavorable contacts with their 5′-terminal phosphates.

because G568 now becomes flexible, allowing dNTP bases and/or templating bases, including Gh, to shift into the DNA minor groove by displacing G568 into the pol interior. These results underscore the need to better elucidate the interrelationships between amino acid side chains within the NBP and bound substrates if we are to understand the mechanism(s) by which DNA pols achieve high-fidelity replication.

REFERENCES

1. Kathe, S. D., Barrantes-Reynolds, R., Jaruga, P., Newton, M. R., Burrows, C. J., Bandaru, V., Dizdaroglu, M., Bond, J. P., and Wallace, S. S. (2009) Plant and fungal Fpg homologs are formamidopyrimidine DNA glycosylases but not 8-oxoguanine DNA glycosylases. *DNA Repair 8*, 643–653.
2. Steenken, S., and Jovanovic, S. V. (1997) How Easily Oxidizable Is DNA? One-Electron Reduction Potentials of Adenosine and Guanosine Radicals in Aqueous Solution. *J. Am. Chem. Soc. 119*, 617–618.
3. Sekiguchi, M., and Tsuzuki, T. (2002) Oxidative nucleotide damage: Consequences and prevention. *Oncogene 21*, 8895–8904.
4. Malins, D. C., and Haimanot, R. (1991) Major alterations in the nucleotide structure of DNA in cancer of the female breast. *Cancer Res. 51*, 5430–5432.
5. Degan, P., Shigenaga, M. K., Park, E. M., Alperin, P. E., and Ames, B. N. (1991) Immunoaffinity isolation of urinary 8-hydroxy-2′-deoxyguanosine and 8-hydroxyguanine and quantitation of 8-hydroxy-2′-deoxyguanosine in DNA by polyclonal antibodies. *Carcinogenesis 12*, 865–871.
6. Steenken, S., Jovanovic, S. V., Bietti, M., and Bernhard, K. (2000) The Trap Depth (in DNA) of 8-Oxo-7,8-dihydro-2′deoxyguanosine as Derived from Electron-Transfer Equilibria in Aqueous Solution. *J. Am. Chem. Soc. 122*, 2372–2374.
7. Yanagawa, H., Ogawa, Y., and Ueno, M. (1992) Redox ribonucleosides. Isolation and characterization of 5-hydroxyuridine, 8-hydroxyguanosine, and 8-hydroxyadenosine from Torula yeast RNA. *J. Biol. Chem. 267*, 13320–13326.
8. Berger, M., Anselmino, C., Mournet, J.-F., and Cadet, J. (1990) High performance liquid chromatography-electrochemical assay for monitoring the formation of 8-oxo-7,8-dihydroadenine and its related 2′-deoxyribonucleoside. *J. Liq. Chromatogr. 13*, 929–940.
9. Burrows, C. J., Muller, J. G., Kornyushyna, O., Luo, W., Duarte, V., Leipold, M. D., and David, S. S. (2002) Structure and potential mutagenicity of new hydantoin products from guanosine and 8-oxo-7,8-dihydroguanine oxidation by transition metals. *Environ. Health Perspect. 110* (Suppl. 5), 713–717.
10. Luo, W., Muller, J. G., Rachlin, E. M., and Burrows, C. J. (2001) Characterization of hydantoin products from one-electron oxidation of 8-oxo-7,8-dihydroguanosine in a nucleoside model. *Chem. Res. Toxicol. 14*, 927–938.
11. Aller, P., Ye, Y., Wallace, S. S., Burrows, C. J., and Doublie, S. (2010) Crystal structure of a replicative DNA polymerase bound to the oxidized guanine lesion guanidinohydantoin. *Biochemistry 49*, 2502–2509.
12. Mishchuk, Y. R., Potyagaylo, D. M., and Hovorun, D. M. (2000) Structure and dynamics of 6-azacytidine by MNDO/H quantum-chemical method. *J. Mol. Struct. 552*, 283–289.
13. Verdolino, V., Cammi, R., Munk, B. H., and Schlegel, H. B. (2008) Calculation of pK_a values of nucleobases and the guanine oxidation products guanidinohydantoin and spiroiminodihydantoin using density functional theory and a polarizable continuum model. *J. Phys. Chem. B 112*, 16860–16873.
14. David, S. S., O'Shea, V. L., and Kundu, S. (2007) Base-excision repair of oxidative DNA damage. *Nature 447*, 941–950.
15. Kornyushyna, O., Berges, A. M., Muller, J. G., and Burrows, C. J. (2002) In vitro nucleotide misinsertion opposite the oxidized guanosine lesions spiroiminodihydantoin and guanidinohydantoin and DNA synthesis past the lesions using *Escherichia coli* DNA polymerase I (Klenow fragment). *Biochemistry 41*, 15304–15314.
16. Kornyushyna, O., and Burrows, C. J. (2003) Effect of the oxidized guanosine lesions spiroiminodihydantoin and guanidinohydantoin on proofreading by *Escherichia coli* DNA polymerase I (Klenow fragment) in different sequence contexts. *Biochemistry 42*, 13008–13018.
17. Duarte, V., Muller, J. G., and Burrows, C. J. (1999) Insertion of dGMP and dAMP during in vitro DNA synthesis opposite an oxidized form of 7,8-dihydro-8-oxoguanine. *Nucleic Acids Res. 27*, 496–502.
18. Tano, K., Iwamatsu, Y., Yasuhira, S., Utsumi, H., and Takimoto, K. (2001) Increased base change mutations at G:C pairs in *Escherichia coli* deficient in endonuclease III and VIII. *J. Radiat. Res. 42*, 409–413.
19. Takimoto, K., Tano, K., Hashimoto, M., Hori, M., Akasaka, S., and Utsumi, H. (1999) Delayed transfection of DNA after riboflavin mediated photosensitization increases G:C to C:G transversions of supF gene in *Escherichia coli* mutY strain. *Mutat. Res. 445*, 93–98.
20. Akasaka, S., and Takimoto, K. (1994) Hydrogen peroxide induces G:C to T:A and G:C to C:G transversions in the supF gene of *Escherichia coli*. *Mol. Gen. Genet. 243*, 500–505.
21. Mcbride, T. J., Schneider, J. E., Floyd, R. A., and Loeb, L. A. (1992) Mutations induced by methylene blue plus light in single-stranded M13mp2. *Proc. Natl. Acad. Sci. U.S.A. 89*, 6866–6870.
22. Schulz, I., Mahler, H.-C., Boiteux, S., and Epe, B. (2000) Oxidative DNA base damage induced by singlet oxygen and photosensitization: Recognition by repair endonucleases and mutagenicity. *Mutat. Res. 461*, 145–156.
23. Garrigue-Antar, L., Munoz-Antonia, T., Antonia, S. J., Gesmonde, J., Vellucci, V. F., and Reiss, M. (1995) Missense mutations of the transforming growth factor β type II receptor in human head and neck squamous carcinoma cells. *Cancer Res. 55*, 3982–3987.
24. Kino, K., and Sugiyama, H. (2005) UVR-induced G-C to C-G transversions from oxidative DNA damage. *Mutat. Res. 571*, 33–42.
25. Hailer, M. K., Slade, P. G., Martin, B. D., Rosenquist, T. A., and Sugden, K. D. (2005) Recognition of the oxidized lesions spiroiminodihydantoin and guanidinohydantoin in DNA by the mammalian base excision repair glycosylases NEIL1 and NEIL2. *DNA Repair 4*, 41–50.

26. Zhao, X., Krishnamurthy, N., Burrows, C. J., and David, S. S. (2010) Mutation versus repair: NEIL1 removal of hydantoin lesions in single-stranded, bulge, bubble, and duplex DNA contexts. *Biochemistry 49*, 1658–1666.
27. Krishnamurthy, N., Zhao, X., Burrows, C. J., and David, S. S. (2008) Superior removal of hydantoin lesions relative to other oxidized bases by the human DNA glycosylase hNEIL1. *Biochemistry 47*, 7137–7146.
28. Wang, T. S., Wong, S. W., and Korn, D. (1989) Human DNA polymerase α: Predicted functional domains and relationships with viral DNA polymerases. *FASEB J. 3*, 14–21.
29. Beckman, J., Wang, M., Blaha, G., Wang, J., and Konigsberg, W. H. (2010) Substitution of Ala for Tyr567 in RB69 DNA polymerase allows dAMP to be inserted opposite 7,8-dihydro-8-oxoguanine. *Biochemistry 49*, 4116–4125.
30. Zhang, H., Rhee, C., Bebenek, A., Drake, J. W., Wang, J., and Konigsberg, W. (2006) The L561A substitution in the nascent base-pair binding pocket of RB69 DNA polymerase reduces base discrimination. *Biochemistry 45*, 2211–2220.
31. Kuchta, R. D., Mizrahi, V., Benkovic, P. A., Johnson, K. A., and Benkovic, S. J. (1987) Kinetic mechanism of DNA polymerase I (Klenow). *Biochemistry 26*, 8410–8417.
32. Maniatis, T., Fritsch, E. F., and Sambrook, J. (1982) Molecular Cloning: A Laboratory Manual, Cold Spring Harbor Laboratory Press, Plainview, NY.
33. Otwinowski, Z., and Minor, W. (1997) Processing of X-ray diffraction data collected in oscillation mode. In Methods in Enzymology (Carter, C. W., and Sweet, R. M., Eds.) pp 307−326, Academic Press, San Diego.
34. Franklin, M. C., Wang, J., and Steitz, T. A. (2001) Structure of the replicating complex of a pol α family DNA polymerase. *Cell 105*, 657–667.
35. Murshudov, G. N., Vagin, A. A., and Dodson, E. J. (1997) Refinement of macromolecular structures by the maximum-likelihood method. *Acta Crystallogr. D53*, 240–255.
36. Navaza, J. (1994) AMoRE: An automated package for molecular replacement. *Acta Crystallogr. A50*, 157–163.
37. Emsley, P., and Cowtan, K. (2004) Coot: Model-building tools for molecular graphics. *Acta Crystallogr. D60*, 2126–2132.
38. Carson, M. (1991) Ribbons 2.0. *J. Appl. Crystallogr. 24*, 958–961.
39. Zhang, H., Beckman, J., Wang, J., and Konigsberg, W. (2009) RB69 DNA polymerase mutants with expanded nascent base-pair-binding pockets are highly efficient but have reduced base selectivity. *Biochemistry 48*, 6940–6950.
40. Aller, P., Rould, M. A., Hogg, M., Wallace, S. S., and Doublie, S. (2007) A structural rationale for stalling of a replicative DNA polymerase at the most common oxidative thymine lesion, thymine glycol. *Proc. Natl. Acad. Sci. U.S.A. 104*, 814–818.
41. Stengel, G., Purse, B. W., Wilhelmsson, L. M., Urban, M., and Kuchta, R. D. (2009) Ambivalent incorporation of the fluorescent cytosine analogues tC and tC^o by human DNA polymerase α and Klenow fragment. *Biochemistry 48*, 7547–7555.
42. Hollenstein, M., Hipolito, C. J., Lam, C. H., and Perrin, D. M. (2009) A self-cleaving DNA enzyme modified with amines, guanidines and imidazoles operates independently of divalent metal cations (M^{2+}). *Nucleic Acids Res. 37*, 1638–1649.
43. Cahova, H., Havran, L., Brazdilova, P., Pivonkova, H., Pohl, R., Fojta, M., and Hocek, M. (2008) Aminophenyl- and nitrophenyl-labeled nucleoside triphosphates: Synthesis, enzymatic incorporation, and electrochemical detection. *Angew. Chem., Int. Ed. 47*, 2059–2062.
44. Liu, H. B., Gao, J. M., Maynard, L., Saito, Y. K., and Kool, E. T. (2004) Toward a New Genetic System with Expanded Dimensions: Size-Expanded Analogues of Deoxyadenosine and Thymidine. *J. Am. Chem. Soc. 126*, 1102–1109.
45. Horhota, A. T., Szostak, J. W., and McLaughlin, L. W. (2006) Glycerol nucleoside triphosphates: Synthesis and polymerase substrate activities. *Org. Lett. 8*, 5345–5347.
46. Xia, G., Chen, L., Sera, T., Fa, M., Schultz, P. G., and Romesberg, F. E. (2002) Directed evolution of novel polymerase activities: Mutation of a DNA polymerase into an efficient RNA polymerase. *Proc. Natl. Acad. Sci. U.S.A. 99*, 6597–6602.
47. Ghadessy, F. J., Ramsay, N., Boudsocq, F., Loakes, D., Brown, A., Iwai, S., Vaisman, A., Woodgate, R., and Holliger, P. (2004) Generic expansion of the substrate spectrum of a DNA polymerase by directed evolution. *Nat. Biotechnol. 22*, 755–759.
48. Loakes, D., and Holliger, P. (2009) Polymerase engineering: Towards the encoded synthesis of unnatural biopolymers. *Chem. Commun.*, 4619–4631.
49. Krishnamurthy, N., Muller, J. G., Burrows, C. J., and David, S. S. (2007) Unusual structural features of hydantoin lesions translate into efficient recognition by *Escherichia coli* Fpg. *Biochemistry 46*, 9355–9365.
50. Bren, U., Martinek, V., and Florian, J. (2006) Free energy simulations of uncatalyzed DNA replication fidelity: Structure and stability of T·G and dTTP·G terminal DNA mismatches flanked by a single dangling nucleotide. *J. Phys. Chem. B 110*, 10557–10566.
51. Fagan, P. A., Fabrega, C., Eritja, R., Goodman, M. F., and Wemmer, D. E. (1996) NMR study of the conformation of the 2-aminopurine: cytosine mismatch in DNA. *Biochemistry 35*, 4026–4033.
52. Sowers, L. C., Boulard, Y., and Fazakerley, G. V. (2000) Multiple structures for the 2-aminopurine-cytosine mispair. *Biochemistry 39*, 7613–7620.
53. Sowers, L. C., Fazakerley, G. V., Eritja, R., Kaplan, B. E., and Goodman, M. F. (1986) Base pairing and mutagenesis: Observation of a protonated base pair between 2-aminopurine and cytosine in an oligonucleotide by proton NMR. *Proc. Natl. Acad. Sci. U.S.A. 83*, 5434–5438.
54. Minnick, D. T., Liu, L., Grindley, N. D., Kunkel, T. A., and Joyce, C. M. (2002) Discrimination against purine-pyrimidine mispairs in the polymerase active site of DNA polymerase I: A structural explanation. *Proc. Natl. Acad. Sci. U.S.A. 99*, 1194–1199.
55. Yoshida, K., Tosaka, A., Kamiya, H., Murate, T., Kasai, H., Nimura, Y., Ogawa, M., Yoshida, S., and Suzuki, M. (2001) Arg660Ser mutation in *Thermus aquaticus* DNA polymerase I suppresses T → C transitions: Implication of wobble base pair formation at the nucleotide incorporation step. *Nucleic Acids Res. 29*, 4206–4214.
56. Freisinger, E., Grollman, A. P., Miller, H., and Kisker, C. (2004) Lesion (in)tolerance reveals insights into DNA replication fidelity. *EMBO J. 23*, 1494–1505.
57. Kincaid, K., Beckman, J., Zivkovic, A., Halcomb, R. L., Engels, J. W., and Kuchta, R. D. (2005) Exploration of factors driving incorporation of unnatural dNTPS into DNA by Klenow fragment (DNA polymerase I) and DNA polymerase α. *Nucleic Acids Res. 33*, 2620–2628.
58. Beckman, J., Kincaid, K., Hocek, M., Spratt, T., Engels, J., Cosstick, R., and Kuchta, R. D. (2007) Human DNA polymerase α uses a combination of positive and negative selectivity to polymerize purine dNTPs with high fidelity. *Biochemistry 46*, 448–460.
59. Morales, J. C., and Kool, E. T. (2000) Functional hydrogen-bonding map of the minor groove binding tracks of six DNA polymerases. *Biochemistry 39*, 12979–12988.
60. Matsuda, S., Leconte, A. M., and Romesberg, F. E. (2007) Minor groove hydrogen bonds and the replication of unnatural base pairs. *J. Am. Chem. Soc. 129*, 5551–5557.
61. Matsuda, S., and Romesberg, F. E. (2004) Optimization of interstrand hydrophobic packing interactions within unnatural DNA base pairs. *J. Am. Chem. Soc. 126*, 14419–14427.
62. Yang, G., Wang, J., and Konigsberg, W. (2005) Base selectivity is impaired by mutants that perturb hydrogen bonding networks in the RB69 DNA polymerase active site. *Biochemistry 44*, 3338–3346.